

# A New Approach to Fault Diagnostics for Permanent Magnet Synchronous Machines Using Electromagnetic Signature Analysis

Yao Da, *Student Member, IEEE*, Xiaodong Shi, *Member, IEEE*, and Mahesh Krishnamurthy, *Member, IEEE*

**Abstract**—This paper proposes a novel approach to health monitoring and multifault detection in permanent magnet synchronous machines using direct flux measurement with search coils. Unlike other spectrum-based fault detection schemes, only the fundamental frequency component of the measured voltage is utilized for fault detection. Therefore, the performance of the proposed scheme is not affected by nonstationary speed or harmonics introduced by the power supply. In addition, location of interturn short circuits and direction of static eccentricity can be detected, which have never been done by any other scheme. In spite of the invasive nature of the technique, it is very suitable for mission-critical applications and emerging applications such as off-shore wind turbines, hybrid vehicle technology, and military applications, where early detection of faults is of paramount importance. 2-D simulations using finite element analysis have been presented to validate the proposed method under different operating conditions. Experimental introduction of stator interturn short circuit, demagnetization, and static eccentricity has been discussed, and the proposed scheme is experimentally implemented to examine its effectiveness.

**Index Terms**—Fault diagnosis, finite element analysis (FEA), permanent magnet synchronous machine (PMSM), search coils.

## I. INTRODUCTION

OVER the past decade, permanent magnet synchronous machines (PMSMs) have gained significant popularity in applications such as wind turbines and electric vehicles, owing to their higher efficiency, high output power to volume ratio, and high torque to current ratio. In these mission-critical applications, an unexpected fault or failure of the machine could lead to very high repair or replacement cost, or even catastrophic system failure. Therefore, a robust and reliable health monitoring and fault-diagnostic approach is desired, which could help in scheduling preventive maintenance to lengthen their lifespan and avoid machine failure.

Manuscript received April 12, 2012; revised September 8, 2012 and October 15, 2012; accepted November 6, 2012. Date of current version January 18, 2013. This work was supported in part by the U.S. Department of Energy under Grant DE-EE 0002979. Recommended for publication by Associate Editor Kennel M. Ralph.

Y. Da is with Regal Beloit Corporation, Fort Wayne, IN 46825 USA (e-mail: yda@hawk.iit.edu).

X. Shi is with Mercedes-Benz R&D North America Inc., Redford, MI 48239 USA (e-mail: xshi4@hawk.iit.edu).

M. Krishnamurthy is with the Department of Electrical and Computer Engineering, Illinois Institute of Technology, Chicago, IL 60647 USA (e-mail: kmahesh@ece.iit.edu).

Color versions of one or more of the figures in this paper are available online at <http://ieeexplore.ieee.org>.

Digital Object Identifier 10.1109/TPEL.2012.2227808

Since offline machine fault detection and diagnostic methods do not allow for frequent testing and are financially impractical, many online methods have been proposed by researchers to reduce maintenance costs and provide more reliable diagnosis. One cost-effective way is based on stator current spectrum, usually called motor current signature analysis (MCSA) [1]–[6]. Specific harmonics in the motor current spectrum can be detected as a signature of a specific type of fault. Since discrete Fourier transform (DFT) does not contain the information about time, for machines operated with a rapidly changing speed profile, short-time Fourier transform (STFT) can be applied to overcome the tradeoff between time and frequency resolution. However, a fixed length of window could result in an inconsistent treatment of different current frequencies [7], and changing motor speed makes it harder to determine harmonic orders. To avoid the dilemma between time resolution and frequency resolution, Rosero *et al.* [7] applied both continuous wavelet transform (CWT) and discrete wavelet transform (DWT) to detect demagnetization faults in a machine running under the nonstationary condition. Espinosa *et al.* [6] have presented the same concept using the Hilbert–Huang transform for detecting demagnetization. A similar method is also used to detect dynamic eccentricity fault in a PMSM [8]. Similar to the current spectrum, indications of several faults are also hidden in noise, vibration, and torque spectra [9]–[13]. However, due to the high cost of accelerometer or torque meter, they are usually only implemented in relative larger machines. The limitations of these frequency analysis-based algorithms are relatively time consuming, and it can be difficult to determine the source of specific harmonics. For a brushless permanent magnet machine, additional harmonic frequencies due to partial demagnetization are the same as dynamic eccentricity signature frequencies [14], and they cannot be distinguished. In reality, not only partial demagnetization, but also other asymmetric problems such load imbalance, misalignment, or oscillating load can produce the same harmonics [15].

Another kind of fault-diagnostic method is based on the electric machine model. Negative/zero sequence current [16], [17], negative/zero sequence impedance [18], or negative/zero sequence voltage [19], [20] are utilized as indicators for fault detection. These indicators are sensitive to machine asymmetry so that faults causing unbalance signals can be detected. However, any asymmetry caused by the machine structure or the power supply's unbalance could affect the accuracy of fault detection. Based on the electric machine model, estimated physical parameters can also be used for online fault diagnosis, such as stator resistance, inductance, rotor inertia, friction, and back

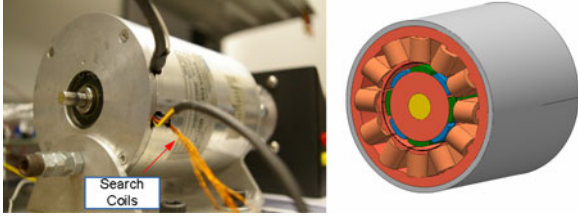


Fig. 1. Test machine and its FEA model.

EMF constant [21]–[24]. In this type of method, usually current, voltage, and speed are measured directly, while other parameters are estimated so that faults can be found from any change in magnitude or asymmetry. However, accurate parameters of a fault-free machine are required. Furthermore, it must be noted that none of these methods discussed previously provide location of the fault.

In this paper, an alternative multifault detection method using search coils is proposed. These coils are wound around armature teeth and, therefore, are invasive in nature, so they typically need to be installed during manufacturing or rewinding. As a matter of fact, search coils are not a new concept at all for electric machine fault detection. Penman *et al.* [25], [26] have developed an approach using a search coil to measure axial leakage flux signal of an induction machine to detect some common faults in induction machines, such as broken rotor bars, wound rotor short circuit, interturn short circuit, eccentric operation, etc. However, they also acknowledge that the technique is not suitable for inverter fed systems due to the additional harmonic content from the power supply, because it is based on spectrum analysis. Neti *et al.* used rotor-mounted search coils to detect stator interturn fault for wound rotor synchronous machines [27] and doubly fed induction machines [28], based on power spectral density of the measured search coil voltage as well. In the proposed method, magnetic flux around the stator is measured using search coils, and only the fundamental frequency components of the measured voltage are utilized for fault detection. So it is immune to high-frequency harmonics, which makes it suitable for inverter/rectifier fed motors or generators, such as wind turbines and automotive systems. In addition, this method does not require the knowledge of machine parameters. Additionally, the exact location of stator winding short circuit and the direction of static eccentricity can be detected.

In order to evaluate the validity of the presented scheme, simulation and experiments have been conducted for a PMSM. Eccentricity, armature winding short-turn, and demagnetization under different load conditions have been modeled by Finite Element Analysis (EFA) and implemented experimentally.

## II. FUNDAMENTALS OF SEARCH COIL IMPLEMENTATION

Fig. 1 presents the test machine utilized in this paper and its FEA model, which is built using a commercial FEA software package MagNet by Infolytica. This three-phase Y-connected machine has a concentrated armature winding and a sinusoidal back EMF.

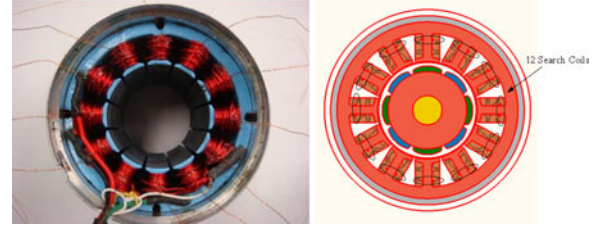


Fig. 2. Implantation of search coils in a test machine and an FEA model.

To allow maximum degrees of freedom during the testing phase, 12 search coils were wound around the stator teeth of this machine, for multifault detection and health monitoring. Four turns are used for each search coil to mitigate the variance between turns for better voltage measurement accuracy. Their implementation is illustrated in Fig. 2. Their voltages were recorded by a data acquisition system for further analysis. Details of the experimental implementation are described in Section VI.

## III. TYPES OF FAULTS IN PM MACHINES

### A. Eccentricity

Eccentricity in a machine is a condition of uneven air-gap between the stator and the rotor. If the condition is severe, the unbalanced magnetic pull (UMP) could cause stator and rotor contact [29]. Generally, eccentricity is classified into three types: static eccentricity, dynamic eccentricity, and mixed eccentricity.

Static eccentricity is the case that there is a displacement of the axis of rotation, which usually could be caused by an oval stator or misaligned mounting of bearings, rotors, or stators. In this case, the air-gap length is fixed in space. The static eccentricity ratio is defined as [30]

$$\vec{\epsilon}_s = \frac{\vec{\epsilon}_s}{g} \quad (1)$$

where  $\epsilon_s$  is the radial distance between rotor axis and stator axis, and  $g$  is the uniform air-gap length. So the eccentricity ratio has the limit as follows:

$$0 \leq |\vec{\epsilon}_s| \leq 1. \quad (2)$$

Dynamic eccentricity is the condition in which the stator axis and the rotor rotation axis are identical, but the rotor's axis is displaced to some degree. Therefore, the minimum air-gap length position rotates around. This case is usually caused by bent shaft, misaligned mounting of bearings, etc. Similarly, the dynamic eccentricity ratio is defined as

$$\vec{\epsilon}_d = \frac{\vec{\epsilon}_d}{g} = \frac{|\vec{\epsilon}_d| \angle \omega_r t}{g} \quad (3)$$

where  $\epsilon_d$  is the radical distance between rotor's axis and stator's axis, and  $\omega_r$  is the mechanical angular speed of the rotor.

Mixed eccentricity is the combination of static and dynamic eccentricity defined by [30]

$$|\vec{\epsilon}_m| = \left| \frac{\vec{\epsilon}_s}{g} + \frac{\vec{\epsilon}_d}{g} \right| = \sqrt{|\vec{\epsilon}_s|^2 + |\vec{\epsilon}_d|^2 + 2|\vec{\epsilon}_s||\vec{\epsilon}_d| \cos(\omega_r t)} \quad (4)$$

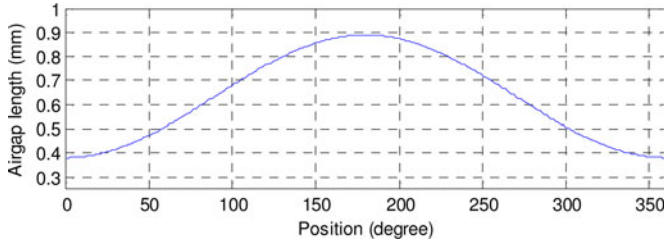


Fig. 3. Static air-gap length around the air-gap.

$$\angle\varphi = \angle\vec{e}_m = \tan^{-1} \frac{|\vec{e}_d| \sin(\omega_r t)}{|\vec{e}_s| + |\vec{e}_d| \cos(\omega_r t)} \quad (5)$$

where  $\varphi$  is the angle of the mixed eccentricity, with a reference to static eccentricity direction. It is a time-dependent variant with a period same as rotor. Thus, the air-gap length  $l_{\text{air}}$  could be calculated as

$$l_{\text{air}}(\zeta, t) = R_s - |\vec{e}_m| g \cos(\zeta - \varphi) - \sqrt{R_r^2 - |\vec{e}_m|^2 g^2 \sin^2(\zeta - \varphi)} \quad (6)$$

where  $\zeta$  is the angular position around the air-gap, from  $0^\circ$  to  $360^\circ$ , while  $R_s$  and  $R_r$  represent stator inside radius and rotor outside radius, respectively. Fig. 3 illustrates the air-gap length as a function of position operating with 40% static eccentricity based on (6), for a PMSM with 0.635 mm (0.025 in) air-gap, 26.924 mm (1.06 in)  $R_s$ , and 26.289 mm (1.035 in)  $R_r$ , at time  $\varphi$  equal to 0.

For dynamic eccentricity air-gap length, it has exactly the same curve but it moves toward one direction at the same speed as the rotor. For mixed eccentricity, the air-gap length is simply the numerical summation of these two minus the average air-gap length.

Magnetic flux is MMF divided by reluctance. In a machine's magnetic circuit, reluctance is a function of the air-gap length and back iron equivalent length  $l_{\text{iron}}$ , as given by

$$\Phi(\zeta, t) = \frac{F_{\text{PM}}}{R_{\text{air}} + R_{\text{iron}}} = \frac{H_{\text{PM}} l_{\text{PM}}}{\frac{l_{\text{air}}(\zeta, t)}{\mu_0 A_{\text{air}}} + \frac{l_{\text{iron}}}{\mu_0 \mu_r A_{\text{iron}}}} \quad (7)$$

where  $\Phi$  is the magnetic flux through a search coil,  $F_{\text{PM}}$  is the MMF produced by a permanent magnet,  $H_{\text{PM}}$  is the H-field of a permanent magnet at its operation point,  $l_{\text{PM}}$  is the thickness of a permanent magnet,  $R_{\text{air}}$  and  $R_{\text{iron}}$  are reluctance of air-gap and back iron, respectively,  $\mu_0$  is the permeability of the air, and  $\mu_r$  is the relative permeability of the back iron. If only static eccentricity exists,  $l_{\text{air}}$  is just a function of position, so  $\Phi$  is also time irrelevant. If dynamic eccentricity exists,  $\Phi$  will be a function of both position and time.

### B. Armature Winding Short Circuit

Armature winding faults are usually caused by insulation failure. They are commonly classified into phase-to-phase short circuit, phase-to-ground short circuit, or interturn short circuit [16]. In a phase-to-phase short circuit, fuses might burn and a machine could stop. In a phase-to-ground short circuit, if a machine still continues to operate, a large torque ripple can be found. In an

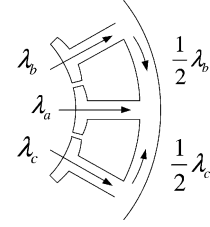


Fig. 4. Flux in teeth and back iron.

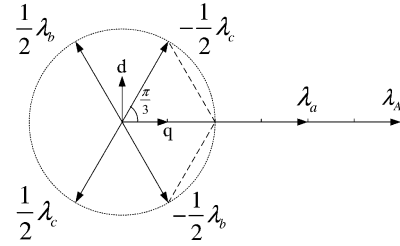


Fig. 5. Three-phase flux linkage vector summation.

interturn short circuit, the faulty winding has a smaller number of effective turns than the other healthy windings, so one can find an asymmetry in machine's armature current or armature MMF. This signature can be used as an indicator in this paper. Fig. 4 shows the path for the coupling of flux when only the armature MMFs are considered.

Applying KCL, one gets

$$\lambda_A = \lambda_a - \frac{1}{2} \lambda_b - \frac{1}{2} \lambda_c \quad (8)$$

where  $\lambda_A$  is the flux linkage through tooth A,  $\lambda_a$  is the flux linkage produced by a coil around tooth A,  $\lambda_b$  is the flux linkage produced by a coil around tooth B, and  $\lambda_c$  is the flux linkage produced by a coil around tooth C. The phasor diagram for this arrangement is shown in Fig. 5. It shows that when a phase-to-ground short circuit occurs at phase A, there is still 1/3 flux linkage remaining, which is produced by adjacent armature windings.

### C. Demagnetization

For permanent magnet machines, field fault typically refers to a failure in the permanent magnets, where demagnetization is the most common issue. The demagnetization could be uniform over all poles or partial over certain region or poles [31]. Conditions that could cause permanent magnets in a PMSM to demagnetize include:

- 1) high operation temperature/cooling system malfunction;
- 2) aging of magnets;
- 3) corrosion of magnets;
- 4) inappropriate armature current.

Commonly used sintered rare-earth magnet materials such as NdFeB and SmCo have straight demagnetization curves in the second quadrant in their B-H loops. The influence of temperature on the magnetic remanence is approximately linear below Curie temperature, which is expressed in

$$B_r(T) = B_r(T_0)[1 + \Delta_B(T - T_0)] \quad (9)$$

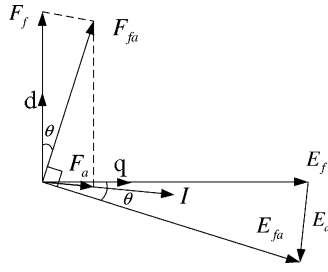


Fig. 6. Phasor/vector diagram for one phase of a PMSM.

where  $T$  is magnet's operation temperature,  $T_0$  is the preferred temperature,  $B_r(T_0)$  is the remanence at  $T_0$ , and  $\Delta_B$  is the reversible temperature coefficient, which is a negative number.

#### IV. OPERATING PRINCIPLES

What each search coil measures is a vector summation of flux due to permanent magnets and armature coil-induced flux, based on an assumption that no saturation occurs. To analyze the reason of flux unbalance, it is required to decouple these two components. The phasor diagram for the operation of the PMSM as a generator is shown in Fig. 6, in which subscripts  $f$ ,  $a$ , and  $fa$  represent field, armature, and the combination of field and armature, respectively.

Under the no-load condition when the rotor revolves at the synchronous speed, voltage  $E_f$  is generated by field MMF  $F_f$  in each phase of the search coil. The MMF distribution can be described as space vectors, while the back EMF are time phasors. Superposition of the field MMF and the armature MMF, known as armature reaction, produces combined MMF  $F_{fa}$ , which is the vector sum of  $F_f$  and  $F_a$ . Additionally, this MMF is responsible for the resultant flux, which induces a back EMF in the search coil under load, denominated as  $E_{fa}$  in Fig. 6.

The PMSM used in the experiment has surface-mounted Nd-FeB permanent magnets, resulting equal  $d$ - $q$  axis inductance. Therefore, phase current is controlled in the same direction of the  $q$  axis. For an interior permanent magnet machine, phase current has a  $d$ -axis component. In either case, a search coil measured voltage can be decoupled as

$$E_{fa}(t) = E_f(t) + E_a(t). \quad (10)$$

Since the PMSM is always controlled by an inverter module, its phase current is never a pure sinusoidal waveform. To get the amplitude of each harmonic, Fourier series transformation is applied into both sides of (10); one can get

$$\sum_{k=-\infty}^{+\infty} a_{fa-k} e^{jk\omega t} = \sum_{k=-\infty}^{+\infty} a_{f-k} e^{jk\omega t} + \sum_{k=-\infty}^{+\infty} a_{a-k} e^{jk\omega t} \quad (11)$$

where  $k$  represents the harmonic order,  $\omega$  represents the fundamental frequency, and  $a$  represents the amplitude of each harmonic.

Just considering its first harmonic, which is the synchronous frequency of the electric machine, one can get

$$a_{fa-1} = a_{f-1} + a_{a-1}. \quad (12)$$

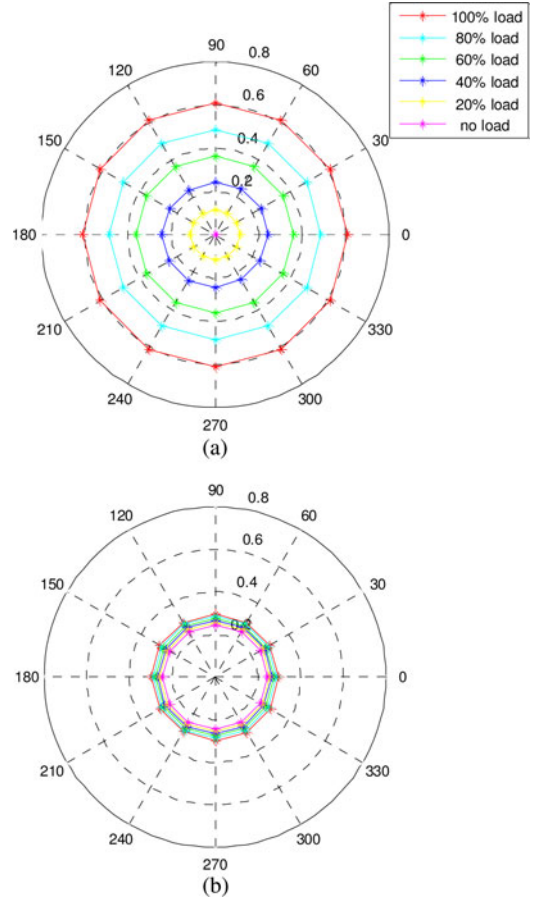


Fig. 7. Decoupled voltage: (a) armature component and (b) field component.

Equation (12) shows that the fundamental component of the measured voltage from the search coil can be decoupled into two components: field and armature components. To acquire amplitude of its first-order harmonic, a linear time-invariant (LTI) filter can be applied to (11). Even though amplitude decay and phase shifting occur during the filtering, the decay ratio and shifting radian are the same for both field and armature components at the same frequency.

#### V. SIMULATION RESULTS

The search coil-mounted PMSM with different fault conditions is simulated using an FEA software package MagNet by Infolytica. This section presents the results from the 2-D FEA simulation.

Voltages measured across the 12 search coils for different load conditions are decoupled and put into two polar graphs, shown in Fig. 7. Fig. 7 is composed of (a) armature reaction voltage and (b) induced field voltage. Each load condition is represented by a different color. There are 12 stars in each curve representing 12 search coils around the 12 stator poles with 30 mechanical degrees between each pair. In this polar figure, the amplitude of the measured coil voltage is denoted by the distance of the star to the polar graph center, in volts.

The two polar graphs in Fig. 7 show that under different load conditions, the armature component voltage is proportional to

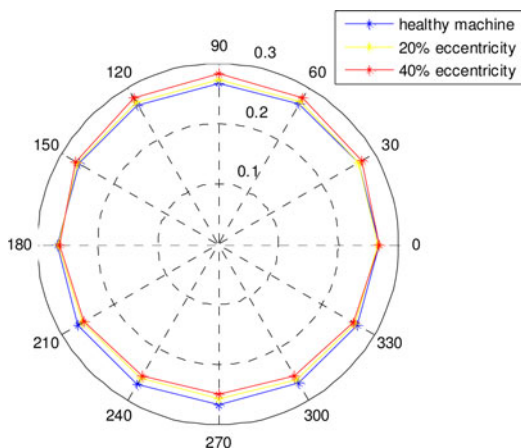


Fig. 8. Field component in a static eccentricity running machine.

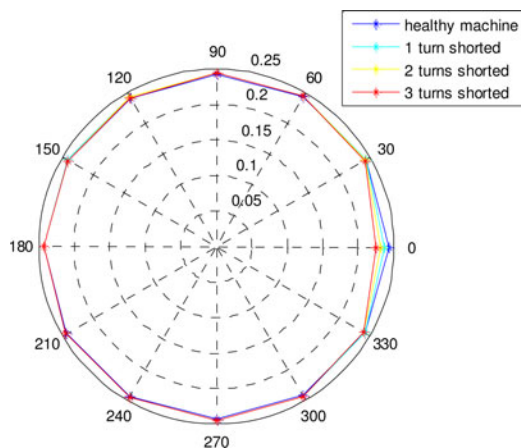


Fig. 10. Armature component in an interturn shorted machine.

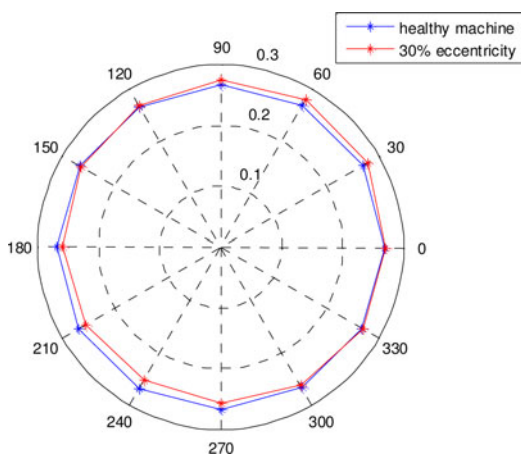


Fig. 9. Field component in a dynamic eccentricity running machine.

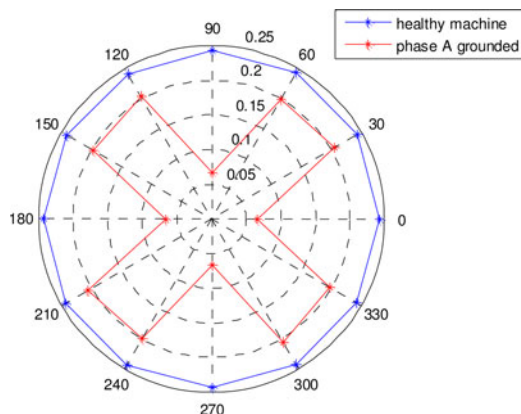


Fig. 11. Armature component in a one-phase grounded machine.

the load while the field component voltage remains the same except some disturbance by the *d*-axis armature-induced MMF.

Fig. 8 shows the field component of the measured voltage of the machine with 0.127 mm (0.005 in, 20%) and 0.254 mm (0.01 in, 40%) static eccentricity, compared with a healthy one. The eccentricity is in the upward direction, which corresponds to 90° in these phasor diagrams. This slight shift to 90° position in this figure can be easily observed.

Fig. 9 illustrates the case with a 30% dynamic eccentricity. It can be seen that there is a shift to 45° position, which is the direction the rotor shifts toward when the data are collected. In the case of dynamic eccentricity, the shift direction rotates at the synchronous speed. Fig. 9 shows the distribution at an arbitrary instant of time.

Fig. 10 shows three cases with one, two, and three turns of the armature coils around a tooth, which is at 0° position, being interturn shorted. A change of ampere-turns at that position causes a distortion of armature MMF. It can be seen that the difference of various number of shorted turns can be distinguished.

Fig. 11 shows the case where one of the three phases is grounded. As explained in Section IV, 1/3 of the magnitude of the flux linkage remains at the teeth of phase A, at the positions 0°, 90°, 180°, and 270°, produced by the neighboring phases,

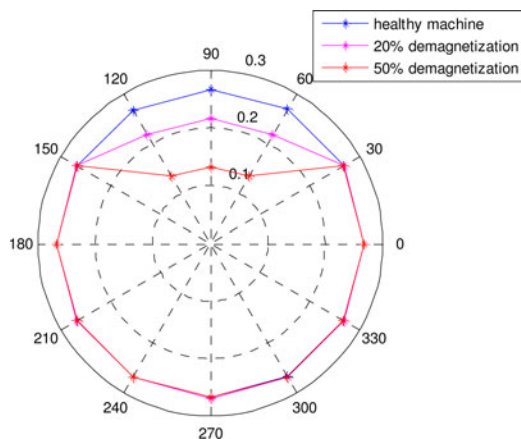


Fig. 12. Field component in a one-pole pair demagnetized machine.

whereas 5/6 of the flux linkage remains at the teeth of phases B and C.

Fig. 12 presents the field component of the measured voltages in a partial demagnetized machine, in which one out of the four pole pairs is 20% and 50% demagnetized, respectively. Since the rotor revolves at synchronous speed, the curves in this figure are time variant, revolving at the synchronous speed while retaining its shape.

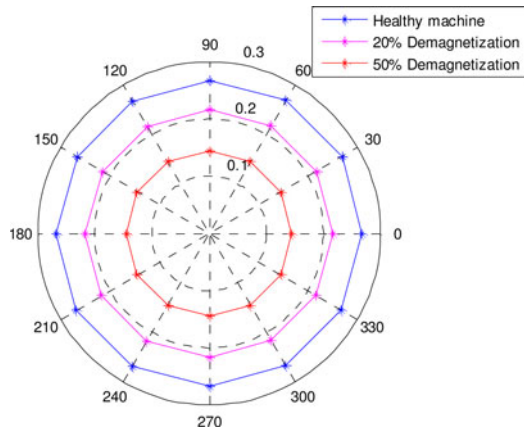


Fig. 13. Field component in a uniform demagnetized machine.

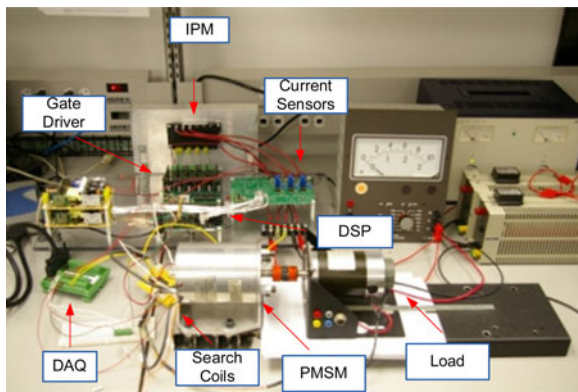


Fig. 14. Experimental set-up.

Fig. 13 presents the field component of the measured voltages at an arbitrarily instant of time in a uniformly demagnetized machine, in which all the poles are 20% and 50% demagnetized, respectively. Since the poles are in uniform demagnetization, even though the red curve in this figure revolves at the synchronous speed, it exhibits the same shape. Therefore, deterioration in magnetic performance of the permanent magnets can be detected from the field component of the coils' measured voltages.

### VI. EXPERIMENTAL VERIFICATION

In order to verify the proposed technique, an experimental setup was implemented, as presented in Fig. 14. A TI DSP TMS320C2812 was used to perform necessary signal processing tasks for vector control, with a PWM frequency of 8 kHz. Current was detected using an LEM current transducer LTS 25-NP for each phase of the machine. A 1000 line incremental encoder was used for position measurement. Voltages of the search coils were monitored using a 16-bit data acquisition system at a sampling frequency of 15 kHz.

The conventional SVPWM vector control technique was implemented to the test set-up. A sample of the search coil measured voltage is shown in Fig. 15.

To experimentally create an interturn short circuit fault, the motor was rewound so that it can switch between two winding

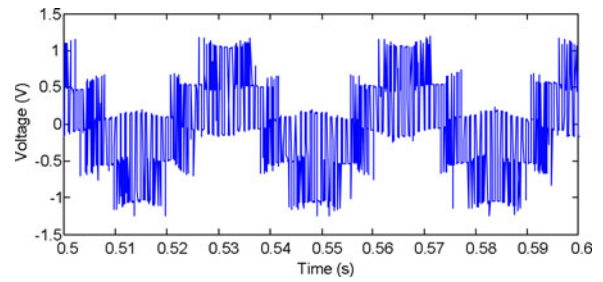


Fig. 15. Measured single search coil voltage.

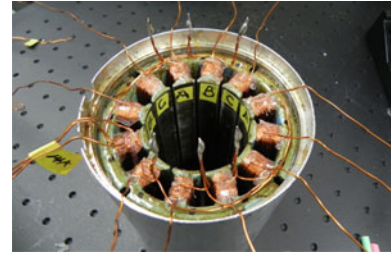


Fig. 16. Rewinding the electric machine to create short turns at phase A.

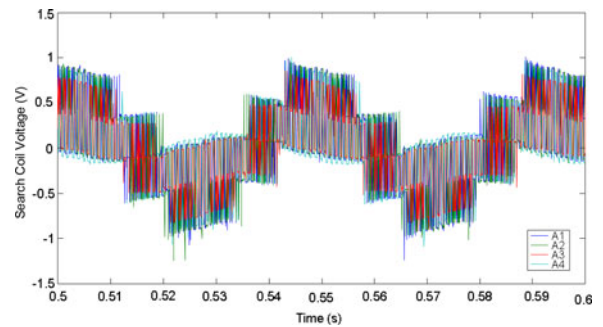


Fig. 17. Search coil voltage from four stator poles of phase A.

modes: the first one fault-free, and another one with four turns shorted in stator tooth A3 in phase A. Fig. 16 shows the stator during the rewinding process.

Fig. 17 shows the search coil voltage from four stator poles of phase A, for the  $q$ -axis current of 0.5 A (vector controlled). There are 4 turns short-circuited (totally 18 turns at each stator pole) at stator pole A3 in that rewind machine. It can be seen that the amplitude of the pulses of A3 (red curve) is smaller than others, which shows that the mutual inductance is smaller than others, indicating a short circuit in the A3 windings. After decoupling, armature component of each search coil voltage is shown in Fig. 18. There are 12 lines representing 12 stator poles in a circle. It can be seen that the armature component of coil A3 is smaller than other ones due to four less turns.

Converting Fig. 18 into the polar graph is shown in Fig. 19. It more explicitly illustrates interturn short circuit fault at the location  $180^\circ$  in the electric machine.

Static eccentricity fault of the motor was also experimentally created in the machine for verification. In order to create a predictable eccentricity, inner slots of the two end plates were ground and two small pieces of electrical tape were put added. This idea is illustrated in Fig. 20.

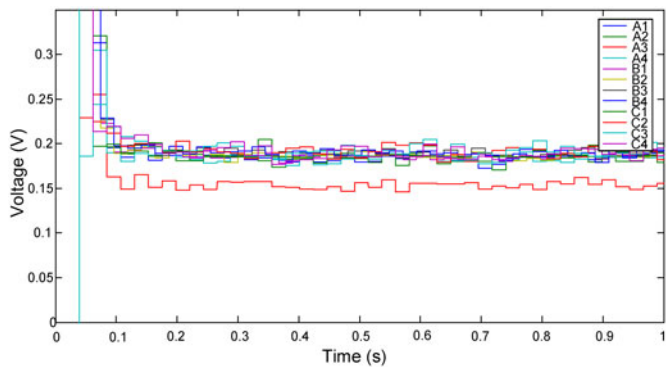


Fig. 18. Armature component of search coil voltage in an interturn shorted machine.

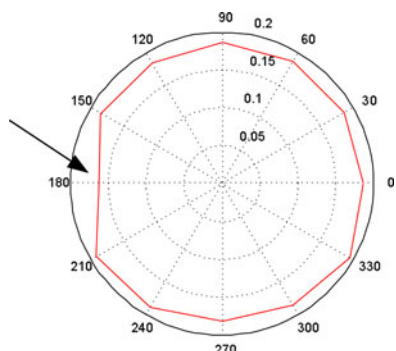


Fig. 19. Armature component of search coil voltage in an interturn shorted machine in a polar graph.

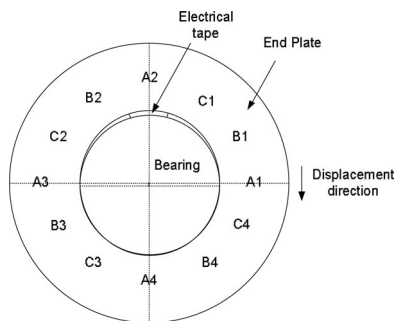


Fig. 20. Illustration of eccentricity.

The air-gap of the machine is 25 mils (0.635 mm), while the displacement of shaft was about 7 mils (the thickness of electrical tape, 0.1778 mm), which gave it about 28% eccentricity. Fig. 21 shows the search coil voltage from four stator poles of phase A, under static eccentricity while the  $q$ -axis current of 0.4 A was applied. In Fig. 22, it can be seen that these four curves have different magnitudes at their fundamental frequency.

After decoupling, field components of the measured voltage from each search coil corresponding to phase A are shown in Fig. 22. It shows that at stator tooth A4 has the highest field component, while A2 has the lowest filed component, and A1 and A3 are in between. This indicates an eccentricity in the direction of A4, which has the smallest air-gap.

Putting together decoupled field components of 12 search coils, voltage in a polar graph clearly highlights the eccentric-

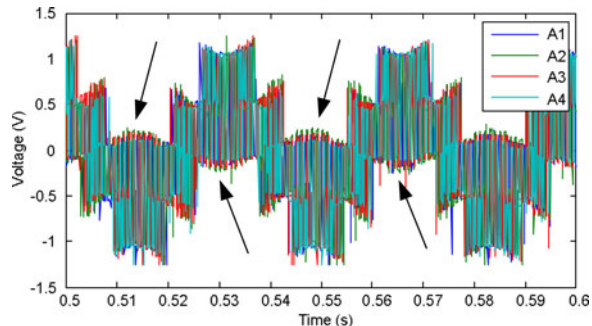


Fig. 21. Search coil voltage from four stator poles of phase A.

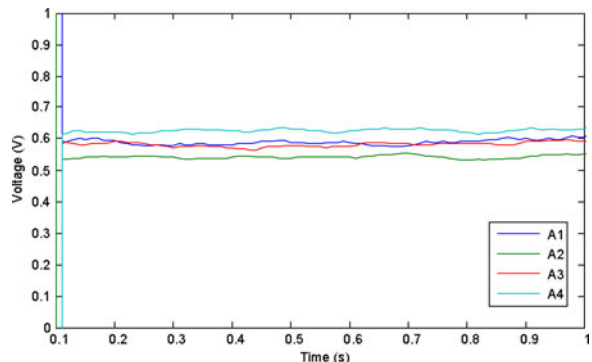


Fig. 22. Field component of search coil voltage in a machine with static eccentricity.

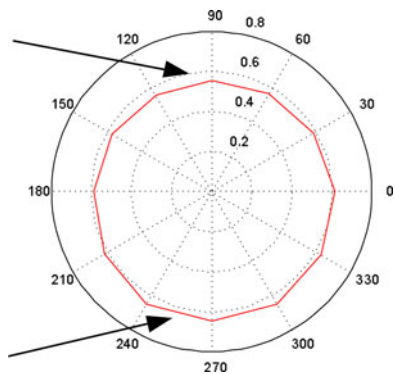


Fig. 23. Field component of search coil voltage in a machine with static eccentricity in a polar graph.

ity toward the lower side of the electric machine, as shown in Fig. 23. Severity of the eccentricity can also be easily observed in this figure.

To experimentally create partial demagnetization, part of one rotor pole was physically removed. The permanent magnets are made with bonded NdFeB. The damaged rotor is shown in Fig. 24, while the result of this damage is shown in Fig. 25. From this figure, it can be seen that one out of the eight rotor poles has approximate 15% less magnetic field.

Fig. 26 shows the search coil voltage from four stator poles of phase A with one pole demagnetized while the  $q$ -axis current of 0.4 A was applied. From Fig. 26, it can be seen that there is an anomaly in the measured voltage every four period for each curve.



Fig. 24. Rotor with a single pole damaged to imitate partial demagnetization.

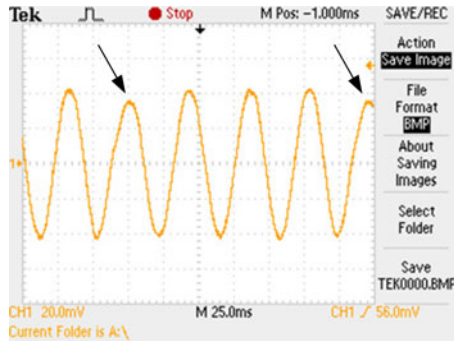


Fig. 25. Back EMF of a single pole demagnetized rotor.

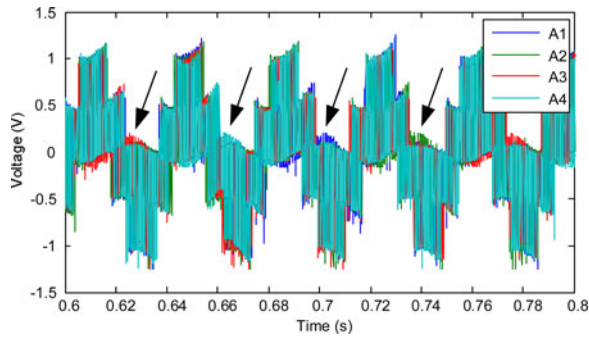


Fig. 26. Search coil voltage from four stator poles of phase A.

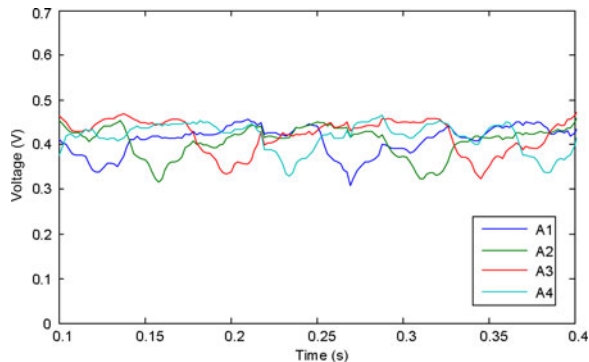


Fig. 27. Field voltage component of search coils in the partial demagnetized machine.

The field component of voltage from each search coil corresponding to phase A is shown in Fig. 27. It can be seen that there is a periodical dip for each curve, which indicates the partial demagnetization of the rotor. Putting together decoupled field components of 12 search coil voltage in a polar graph Fig. 28, partial demagnetization can be observed clearly.

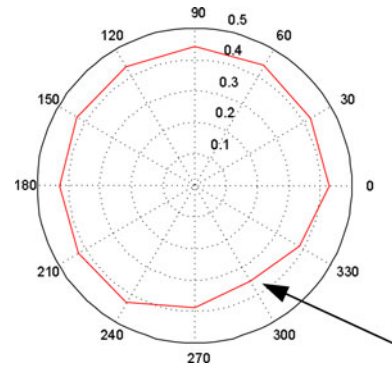


Fig. 28. Field component of search coil voltage in a machine with partial demagnetization in a polar graph.

## VII. CONCLUSION

In this paper, a novel scheme for PMSM health monitoring and fault diagnosis has been proposed. Search coils are wound around each tooth so that the air-gap flux density can be measured. Although the method is invasive, only the first-order harmonic is used for fault detection so that it is immune to the harmonics induced by power electronic devices. Another benefit of this technique is that the load condition does not necessarily need to be specified for accurate fault diagnosis.

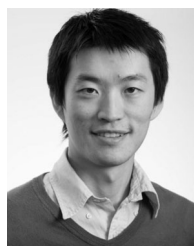
2-D time transient FEA simulations have been presented for the validation of the proposed method over different motor operation conditions. The faults considered in this study include static and dynamic eccentricity, interturn short circuit, phase-to-ground short circuit, and partial and uniform demagnetization. Results show that the signatures of different faults are easy to identify, so no time-consuming pattern recognition algorithm is required. Furthermore, the direction of eccentricity and the location of winding shorted turns can be found. In addition, this method is also capable of evaluating the severity of each fault, which is of significant importance in mission-critical applications such as automotive, aerospace, and military.

Because of the invasive nature of the technique, it is not aimed for machines that have already been deployed. At the same time, it must be noted that the increase in cost is not significant if search coils are installed during the machine manufacturing or rewinding stage, since they are just thin copper wires. For high-power commercial and industrial applications, system reliability is usually of more concern than cost, which makes this technique a very effective tool for condition monitoring and fault detection.

## REFERENCES

- [1] R. R. Schoen, T. G. Habetler, F. Kamran, and R. G. Bartfield, "Motor bearing damage detection using stator current monitoring," *IEEE Trans. Ind. Appl.*, vol. 31, no. 6, pp. 1274–1279, Dec. 1995.
- [2] G. M. Joksimovic and J. Penman, "The detection of inter-turn short circuits in the stator windings of operating motors," *IEEE Trans. Ind. Electron.*, vol. 47, no. 5, pp. 1078–1084, Oct. 2000.
- [3] W. le Roux, R. G. Harley, and T. G. Habetler, "Detecting rotor faults in low power permanent magnet synchronous machines," *IEEE Trans. Power Electron.*, vol. 22, no. 1, pp. 322–328, Jan. 2007.
- [4] I. P. Georgakopoulos, E. D. Mitronikas, and A. N. Safacas, "Detection of induction motor faults in inverter drives using inverter input current

- analysis," *IEEE Trans. Ind. Electron.*, vol. 58, no. 9, pp. 4365–4373, Sep. 2011.
- [5] B. M. Ebrahimi and J. Faiz, "Feature extraction for short-circuit fault detection in permanent-magnet synchronous motors using stator-current monitoring," *IEEE Trans. Power Electron.*, vol. 25, no. 10, pp. 2673–2682, Oct. 2010.
- [6] A. G. Espinosa, J. A. Rosero, J. Cusido, L. Romeral, and J. A. Ortega, "Fault detection by means of Hilbert–Huang transform of the stator current in a PMSM with demagnetization," *IEEE Trans. Energy Convers.*, vol. 25, no. 2, pp. 312–318, Jun. 2010.
- [7] J.-R. R. Ruiz, J. A. Rosero, A. G. Espinosa, and L. Romeral, "Detection of demagnetization faults in permanent-magnet synchronous motors under nonstationary conditions," *IEEE Trans. Magn.*, vol. 45, no. 7, pp. 2961–2969, Jul. 2009.
- [8] W. Yang, P. J. Tavner, and M. Wilkinson, "Condition monitoring and fault diagnosis of a wind turbine with a synchronous generator using wavelet transforms," in *Proc. 4th IET Conf. Power Electron., Mach. Drives*, 2008, pp. 6–10.
- [9] G.-H. Kang, Y.-D. Son, and G.-T. Kim, "The noise and vibration analysis of BLDC motor due to asymmetrical permanent-magnet overhang effects," *IEEE Trans. Ind. Appl.*, vol. 44, no. 5, pp. 1569–1577, Sep./Oct. 2008.
- [10] T. Yoon, "Magnetically induced vibration in a permanent-magnet brushless DC motor with symmetric pole-slot configuration," *IEEE Trans. Magn.*, vol. 41, no. 6, pp. 2173–2179, Jun. 2005.
- [11] H.-S. Ko and K.-J. Kim, "Characterization of noise and vibration sources in interior permanent-magnet brushless DC motors," *IEEE Trans. Magn.*, vol. 40, no. 6, pp. 3482–3489, Nov. 2004.
- [12] R. A. Leonhard and W. T. Thompson, "Vibration and stray flux monitoring for unbalanced supply and inter-turn winding fault diagnosis in induction machines," *Brit. J. Non-Destruct. Test.*, vol. 28, pp. 211–215, Jul. 1986.
- [13] D. Filbert, "Intelligent measurement methods in technical diagnosis and quality assurance—A comparison," *Measurement*, vol. 6, no. 2, pp. 69–74, Jun. 1988.
- [14] S. Rajagopalan, W. Roux, T. G. Habetler, and R. G. Harley, "Dynamic eccentricity and demagnetized rotor magnet detection in trapezoidal flux (brushless DC) motors operating under different load conditions," *IEEE Trans. Power Electron.*, vol. 22, no. 5, pp. 2061–2069, Sep. 2007.
- [15] J. Hong, D. Hyun, S. Lee, J. Yoo, and K. Lee, "Automated monitoring of magnet quality for permanent magnet synchronous motors at standstill," in *Proc. Energy Convers. Congr. Expo.*, 2009, pp. 2326–2333.
- [16] G. B. Kliman, W. J. Premerlani, R. A. Koegl, and D. Hoeweler, "A new approach to on-line turn fault detection in AC motors," in *Proc. IEEE 31st IAS Annu. Meet., Ind. Appl. Conf.*, 1996, vol. 1, pp. 687–693.
- [17] J. L. Kohler, J. Sottile, and F. C. Trutt, "Alternatives for assessing the electrical integrity of induction motors," *IEEE Trans. Ind. Appl.*, vol. 28, no. 5, pp. 1109–1117, Oct. 1992.
- [18] J. Sottile and J. L. Kohler, "An on-line method to detect incipient failure of turn insulation in random-wound motors," *IEEE Trans. Energy Convers.*, vol. 8, no. 4, pp. 762–768, Dec. 1993.
- [19] M. A. Cash, T. G. Habetler, and G. B. Kliman, "Insulation failure prediction in AC machines using line-neutral voltages," *IEEE Trans. Ind. Appl.*, vol. 34, no. 6, pp. 1234–1239, Dec. 1998.
- [20] J. Urresty, J.-R. Riba, M. Delgado, and L. Romeral, "Detection of demagnetization faults in surface-mounted permanent magnet synchronous motors by means of the zero-sequence voltage component," *IEEE Trans. Energy Convers.*, vol. 27, no. 1, pp. 42–51, Mar. 2012.
- [21] D. Filbert, "Advanced fault diagnosis for the mass production of small-power electric motors," in *Proc. SPIE*, Sep. 1993, vol. 2101, no. 1, pp. 100–110.
- [22] C. Schneider and D. Filbert, "Parameter estimation and residual analysis a comparison," in *Proc. IFAC Fault Detect., Supervis. Safety Tech. Processes*, Jun. 1994, pp. 701–705.
- [23] X. Liu, H. Zhang, J. Liu, and J. Yang, "Fault detection and diagnosis of permanent-magnet DC motor based on parameter estimation and neural network," *IEEE Trans. Ind. Electron.*, vol. 47, no. 5, pp. 1021–1030, Oct. 2000.
- [24] J. Hong, S. B. Lee, C. Kral, and A. Haumer, "Detection of airgap eccentricity for permanent magnet synchronous motors based on the d-axis inductance," *IEEE Trans. Power Electron.*, vol. 27, no. 5, pp. 2605–2612, May 2012.
- [25] J. Penman, M. N. Dey, A. J. Tait, and W. E. Bryan, "Condition monitoring of electrical drives," in *IEE Proc. B Electr. Power Appl.*, May 1986, vol. 133, no. 3, pp. 142–148.
- [26] J. Penman, H. G. Sedding, B. A. Lloyd, and W. T. Fink, "Detection and location of interturn short circuits in the stator windings of operating motors," *IEEE Trans. Energy Convers.*, vol. 9, no. 4, pp. 652–658, Dec. 1994.
- [27] P. Neti and S. Nandi, "Stator interturn fault detection of synchronous machines using field current and rotor search-coil voltage signature analysis," *IEEE Trans. Ind. Appl.*, vol. 45, no. 3, pp. 911–920, Jun. 2009.
- [28] D. Shah, S. Nandi, and P. Neti, "Stator-interturn-fault detection of doubly fed induction generators using rotor-current and search-coil-voltage signature analysis," *IEEE Trans. Ind. Appl.*, vol. 45, no. 5, pp. 1831–1842, Oct. 2009.
- [29] C. Kral, T. G. Habetler, and R. G. Harley, "Detection of mechanical imbalances of induction machines without spectral analysis of time-domain signals," *IEEE Trans. Ind. Appl.*, vol. 40, no. 4, pp. 1101–1106, Aug. 2004.
- [30] B. M. Ebrahimi, J. Faiz, and M. J. Roshtkhari, "Static-, dynamic-, and mixed-eccentricity fault diagnoses in permanent-magnet synchronous motors," *IEEE Trans. Ind. Electron.*, vol. 56, no. 11, pp. 4727–4739, Nov. 2009.
- [31] J. Farooq, S. Srairi, A. Djerdir, and A. Miraoui, "Use of permeance network method in the demagnetization phenomenon modeling in a permanent magnet motor," *IEEE Trans. Magn.*, vol. 42, no. 4, pp. 1295–1298, Apr. 2006.



**Yao Da** (S'08) received the B.S. degree in biomedical engineering from the Southeast University, Nanjing, China, in 2007, and the M.S. and Ph.D. degrees in electrical engineering from the Illinois Institute of Technology, Chicago, in 2009 and 2012, respectively.

He is currently a Power Electronics Design Engineer with Regal Beloit Corporation, Fort Wayne, IN. His research interests include electric machine design, motor driver design, and development of motor control algorithms.



**Xiaodong Shi** (S'09–M'12) received the B.S. and M.S. degrees from the East China University of Science and Technology, Shanghai, China, in 2006 and 2009, respectively, and the Ph.D. degree from the Illinois Institute of Technology, Chicago, in 2012, all in electrical engineering.

He is currently an Electrical Engineer at Mercedes-Benz R&D North America Inc., Redford, MI. His research interests include power electronics and motor drives.



**Mahesh Krishnamurthy** (S'97–M'08) received the M.S. degree from the Missouri University of Science and Technology (formerly University of Missouri at Rolla), Rolla, and the Ph.D. degree from the University of Texas at Arlington, Arlington, in 2004 and 2008, respectively, both in electrical engineering.

He is currently an Assistant Professor of Electrical Engineering and the Director of the Electric Drives and Energy Conversion Laboratory at the Illinois Institute of Technology (IIT), Chicago. Before joining IIT, he was a Design Engineer at EF Technologies,

Arlington. He has coauthored more than 50 scientific articles, book chapters, and technical reports. He holds one U.S. patent with two pending. His research primarily focuses on design, analysis, and control of power electronics, electric machines, and adjustable speed drives for renewable energy and automotive applications.

Dr. Krishnamurthy received the 2006–2007 IEEE-VTS Transportation Electronics Fellowship Award for his contributions and is a Distinguished Lecturer with the IEEE-Vehicular Technology Society. He was the Program Co-chair for the 2011 Vehicle Power and Propulsion Conference and is the Technical Program Chair for the 2013 IEEE Transportation Electrification Conference and Exposition. He is also currently serving as a Guest Editor for the Special Section of the IEEE TRANSACTIONS ON VEHICULAR TECHNOLOGY on Sustainable Transportation Systems, and as a Guest Associate Editor for the Special Issue of the IEEE TRANSACTIONS ON POWER ELECTRONICS on Transportation Electrification and Vehicle Systems.